Electronic Supplementary Information

Tin Nanoparticles Decorated Copper Oxide Nanowires for Selective Electrochemical Reduction of Aqueous CO_2 to CO

Yong Zhao, Caiyun Wang*, Gordon G. Wallace*

Intelligent Polymer Research Institute, ARC Centre of Excellence for Electromaterials Science, AIIM, Innovation Campus, University of Wollongong, North Wollongong, NSW 2522, Australia

* Corresponding authors: caiyun@uow.edu.au, gwallace@uow.edu.au

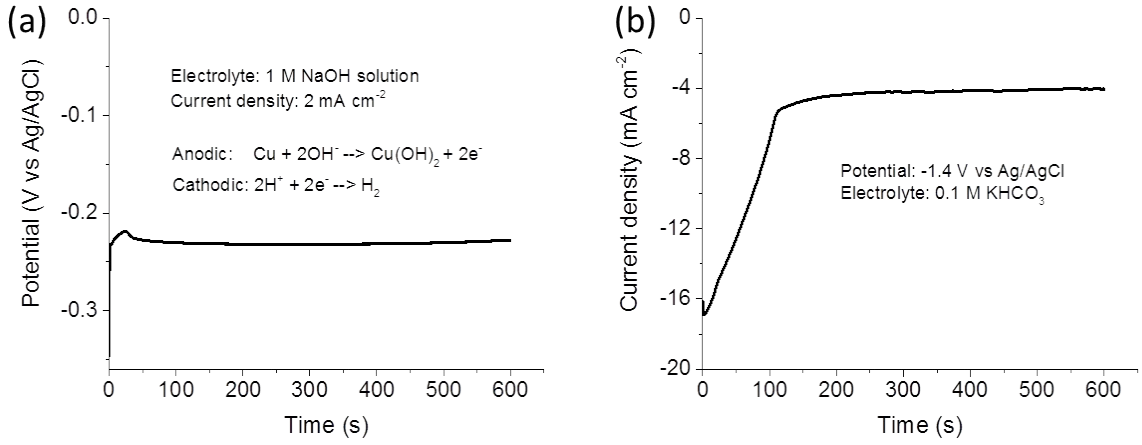

Figure S1 (a) Chronopotentiometry curve for anodizing Cu foil in 1 M NaOH solution; (b) Chronoamperometry curve for the reduction of brown CuO NWs for 10 min at a potential of -1.4 V (vs Ag/AgCl) under Ar atmosphere.

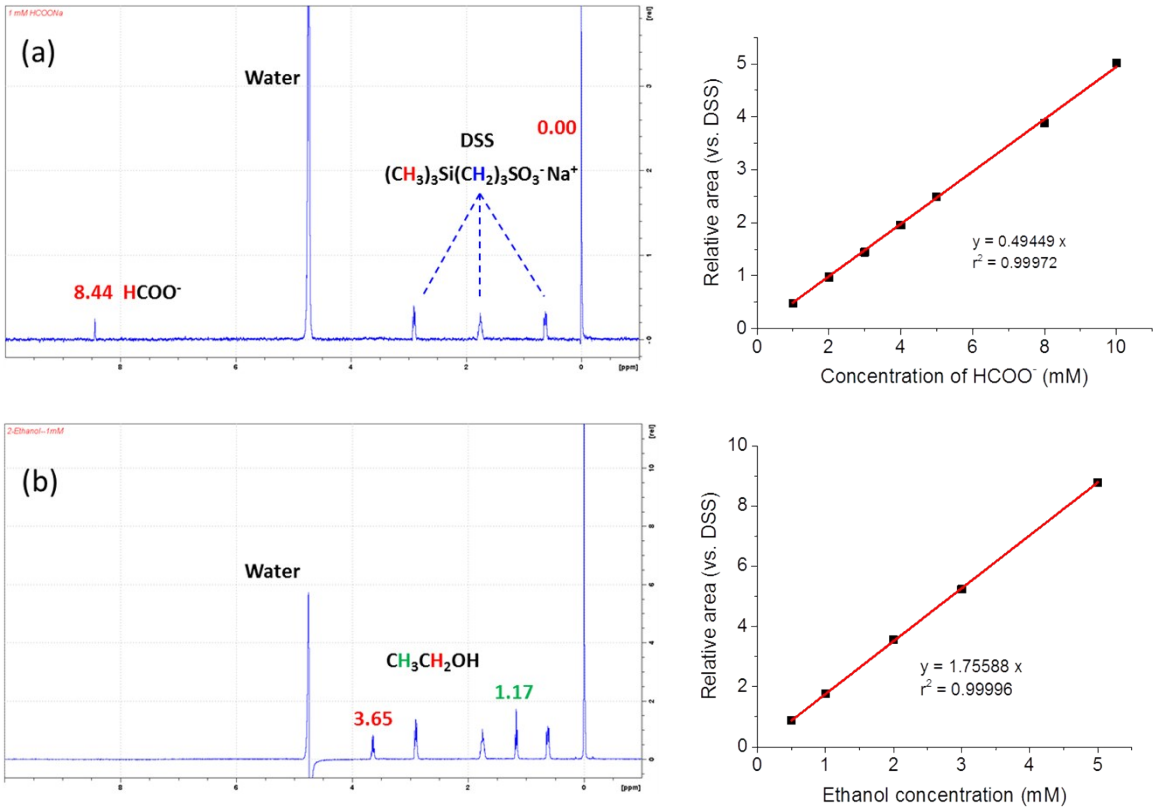

Figure S2 (a) ^{1}H-NMR spectrum for formate (1 mM) and the linear relationship between the formate concentration and relative area vs. DSS; (b) ^{1}H-NMR spectrum for ethanol (1 mM) and the linear relationship between the ethanol concentration and relative area vs. DSS. The relative areas were calculated based on the following equations:

$$Relative\ area(Formate) = \frac{Singlet\ peak\ area\ at\ 8.44\ ppm\ (Formate)}{Peak\ area\ at\ 0.00\ ppm\ (DSS)}$$

$$Relative\ area(Ethanol) = \frac{Triplet\ peak\ area\ at\ 1.17\ ppm\ (Ethanol)}{Peak\ area\ at\ 0.00\ ppm\ (DSS)}$$

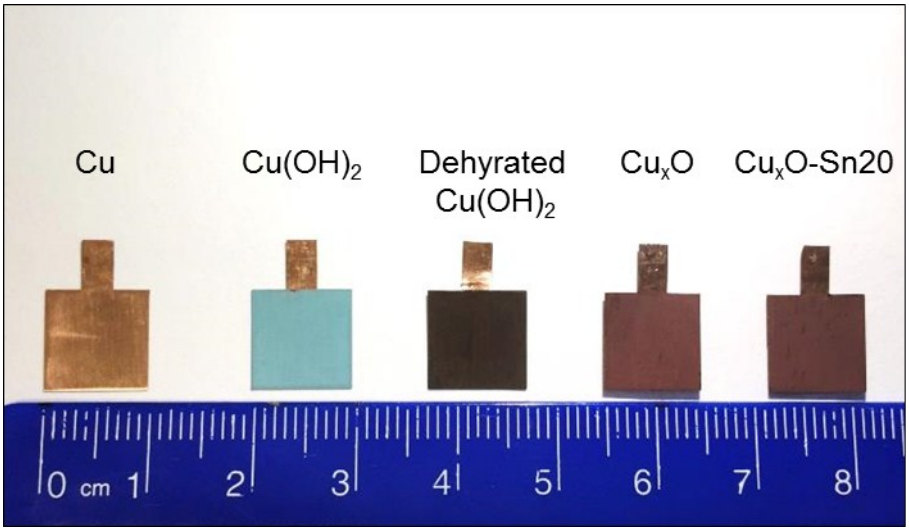

Figure S3 Digital images of Cu foil, $Cu(OH)_2$, dehydrated $Cu(OH)_2$, Cu_xO and Cu_xO-Sn20 NWs.

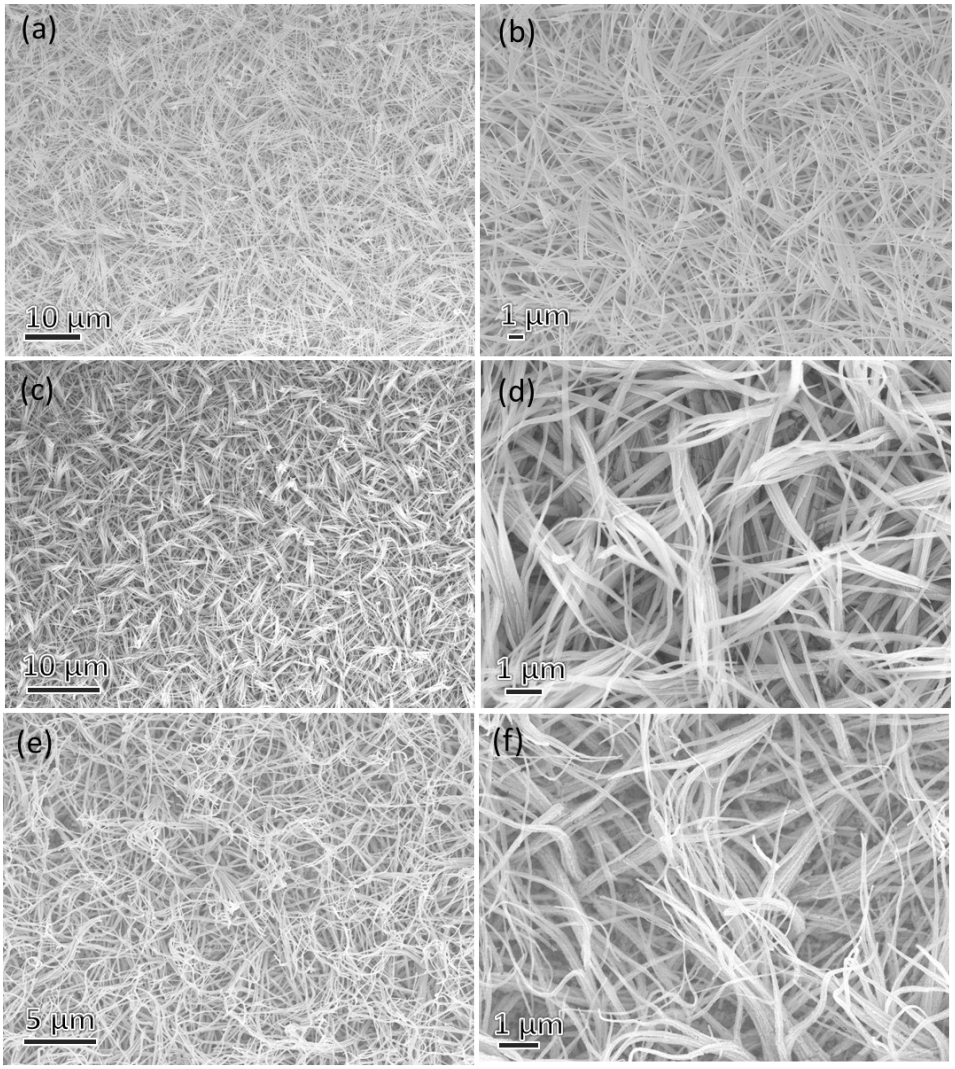

Figure S4 SEM images of (a, b) $Cu(OH)_2$, (c, d) dehydrated $Cu(OH)_2$ and (e, f) Cu_xO under different magnifications. After dehydration by annealing at 200 ℃ in air, the thin nanowires tend to aggregate together, forming nanowire bundles. After the electrochemical reduction in 0.1 M $KHCO_3$ solution for 10 min, the dehydrated $Cu(OH)_2$ NWs were bended and the surfaces became rough, but no aggregation was observed in the interspace of the nanowires. Based on XRD analysis, the as-obtained nanowires are mixtures of CuO and Cu_2O, cited as Cu_xO.

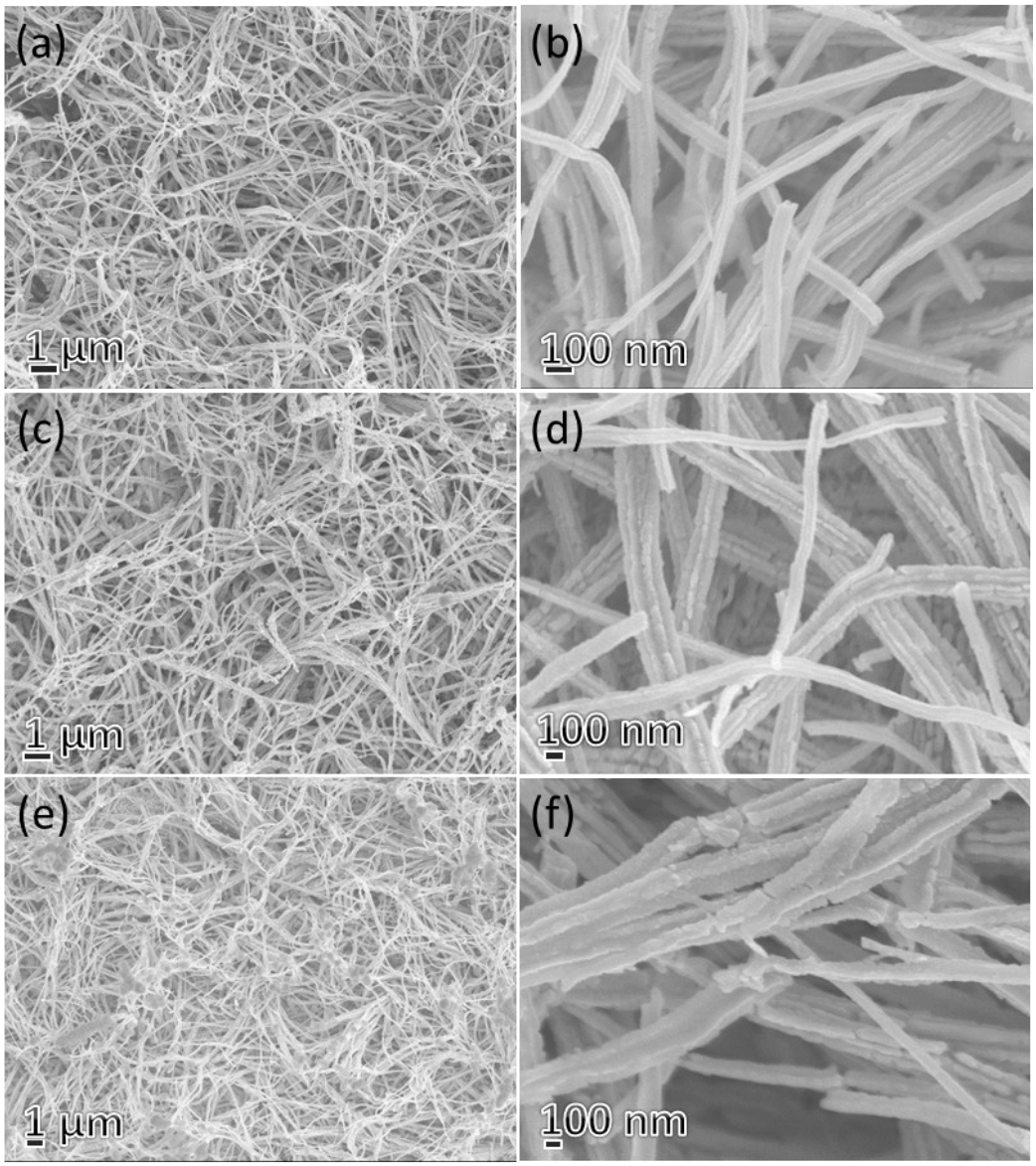

Figure S5 SEM images of Cu_xO-Sn NWs with different Sn deposition time: (a, b) Cu_xO-Sn5s; (c, d) Cu_xO-Sn40s; (e, f) Cu_xO-Sn80s. In figure (e), it can be seen that some aggregates were formed on some nanowire buddles when the deposition time reached 80 s.

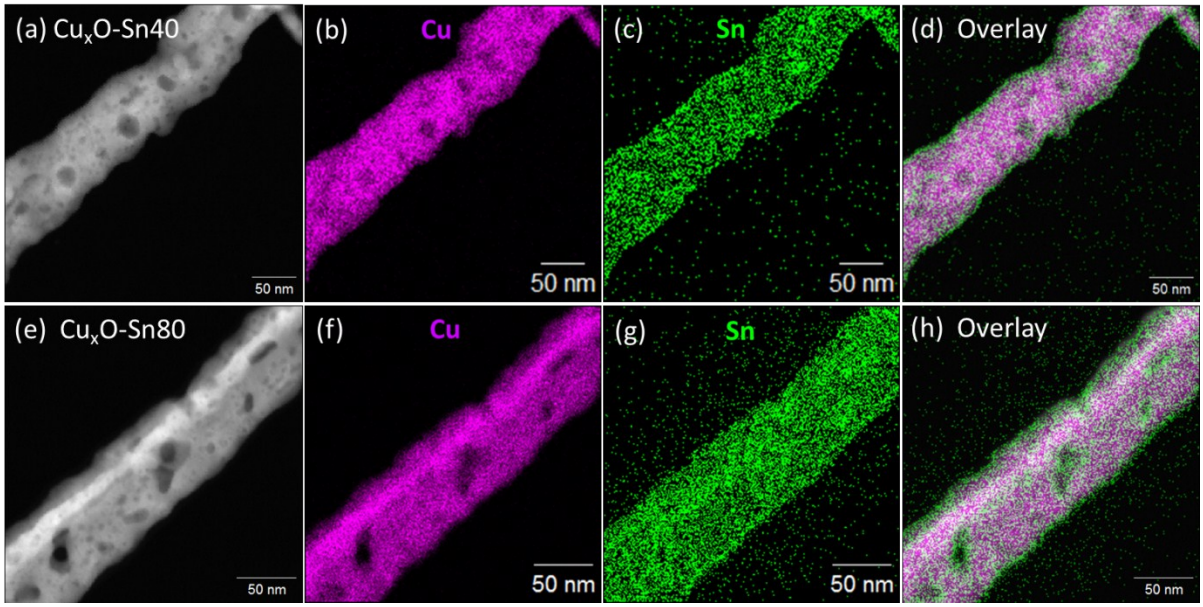

Figure S6 HAADF-STEM image and the corresponding elemental mapping of Cu_xO-Sn40 and Cu_xO-Sn80 NWs. It is clear that the Sn coverage on the surface of Cu_xO NWs increases with the prolonged deposition time. Although some Sn aggregates were formed on some nanowire buddles as shown in Figure S5 (e), the coverage of Sn NPs was still uniform on the surfaces of Cu NWs.

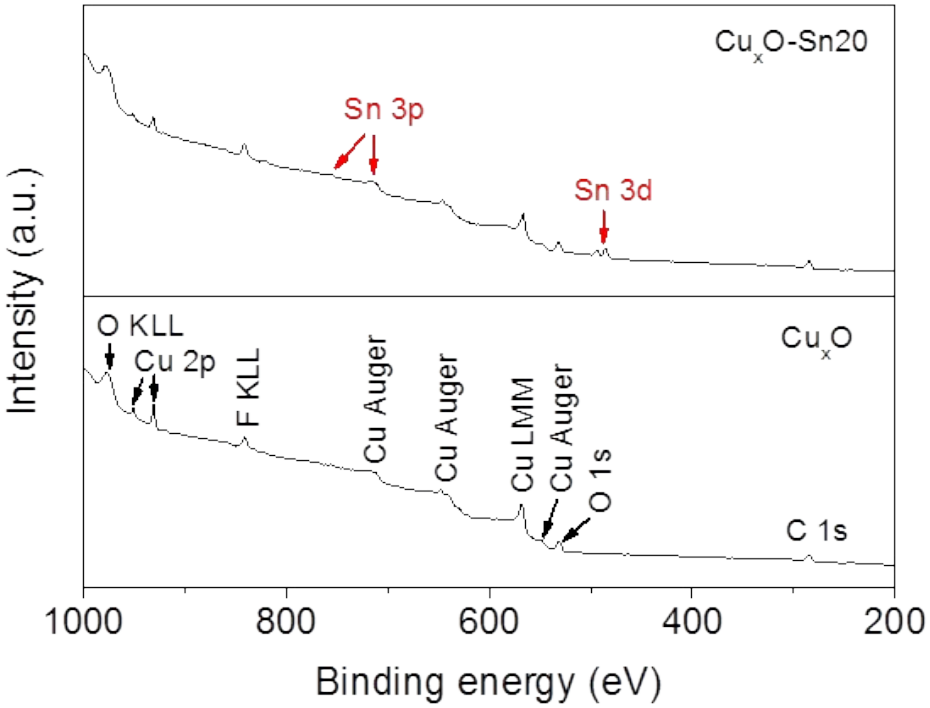

Figure S7 XPS survey spectra of Cu_xO NWs and Cu_xO-Sn20 hybrid NWs.

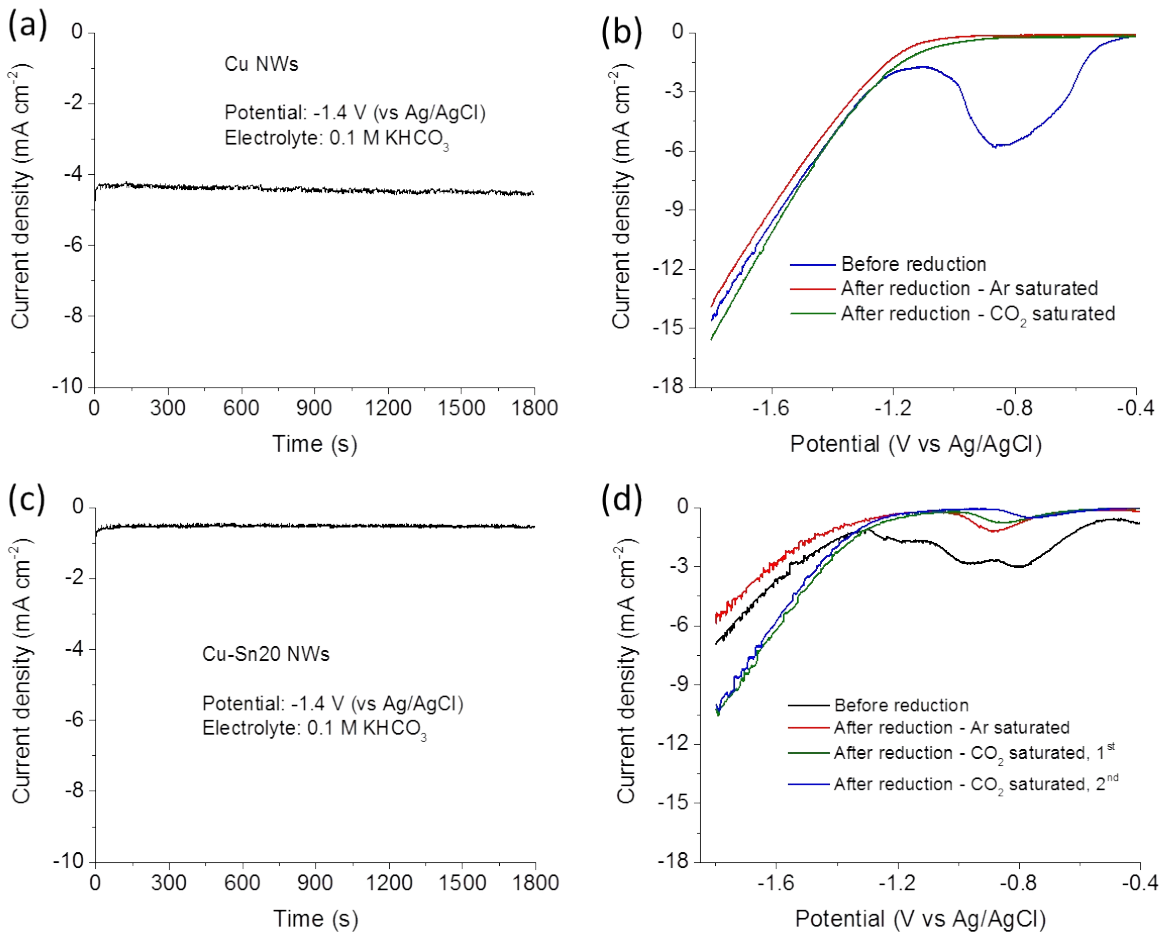

Figure S8 Chronoamperometry curve for pre-reduction of Cu NWs (a) and Cu-Sn20 NWs (c) at -1.4 V (vs Ag/AgCl) in Ar-satured 0.1 M $KHCO_3$ solution. (b) and (d) are the corresponding linear sweep voltammetry before and after pre-reduction in Ar. For Cu NWs, the oxide peak was totally removed after the pre-reduction for 30 min at -1.4 V under Ar. For Cu-Sn20 NWs, the oxide peak still persisted after the pre-reduction, and became gradually decreased with the further increasing cathodic scanning times.

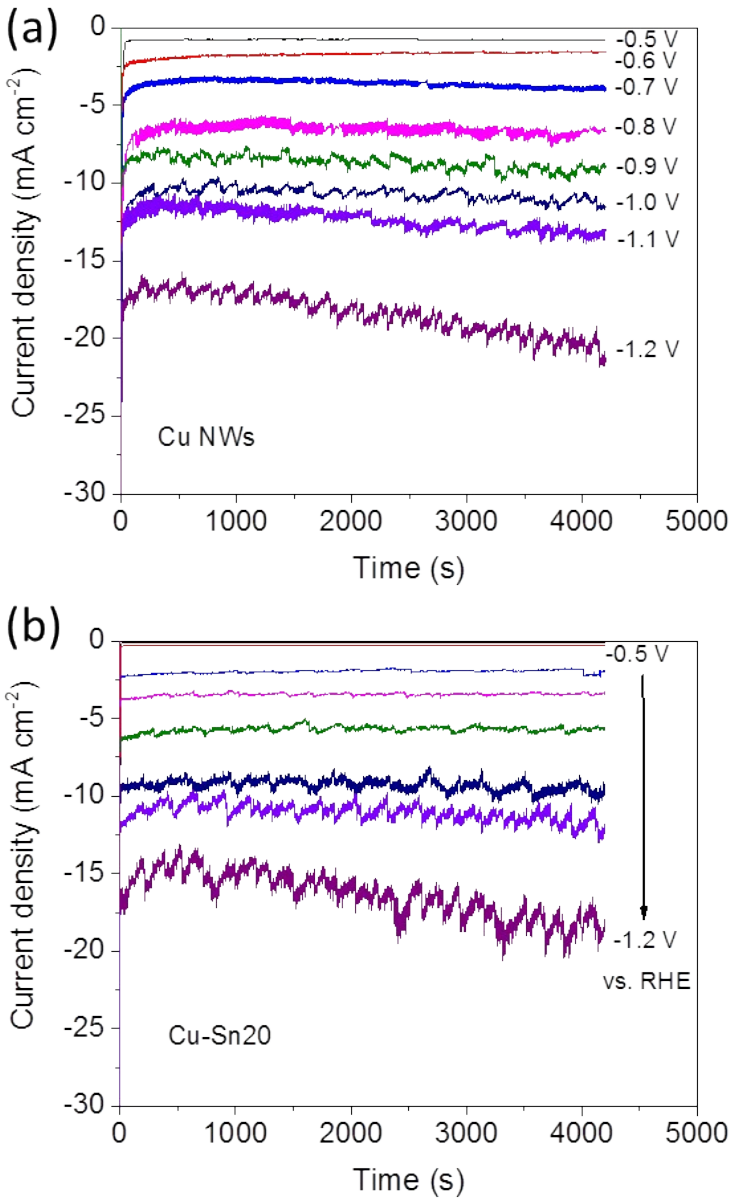

Figure S9 Representative CO_2 electroreduction curves at various potentials in CO_2-satured 0.1 M $KHCO_3$ solution for Cu NWs (a) and Cu-Sn20 NWs (b). It can be seen that after incorporation of Sn NPs, the total current density is slightly depressed. The increase of current density during the CO_2ER under different applied potentials, especially at -1.2 V (vs RHE), may be caused by the enhancing electron transfer due to the further reduction of Cu_xO nanowires under this condition.

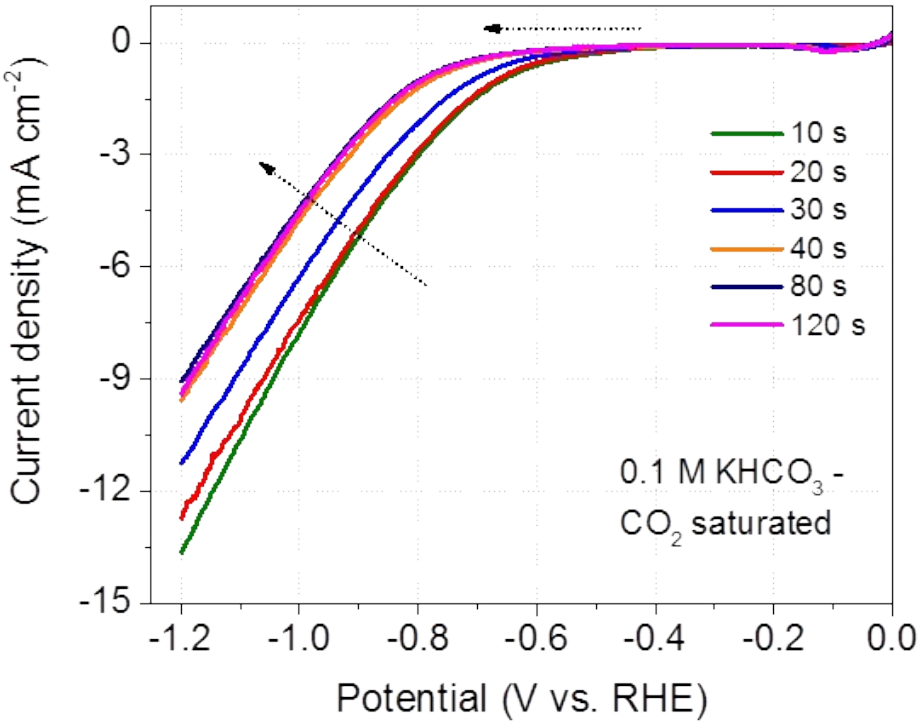

Figure S10 Linear sweep voltammetry (LSV) of Cu-Sn NWs with different Sn deposition time ranging from 10 s to 120 s in CO_2-saturated 0.1 M $KHCO_3$ at a scan rate of 20 mV s^{-1} in the cathodic direction. With the increase of Sn deposition time, the total current density and the onset potential slightly changed. There is an obvious difference between the LSV curves with a deposition time "≤ 30 s" and "> 30 s". For those "≤ 30 s" samples, the total current increases and the onset potential decreases with the increase of Sn deposition time. For the "> 30 s" samples, no big difference in current density and onset potential was observed. This trend is consistent with that of the CO faradaic efficiency and partial current density as a function of Sn deposition time in **Figure 5**.

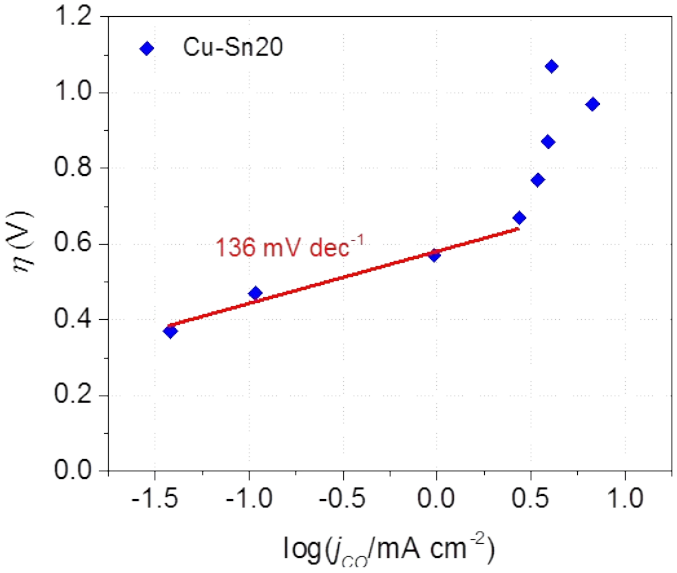

Figure S11 Tafel plot for the Cu-Sn20 electrode.

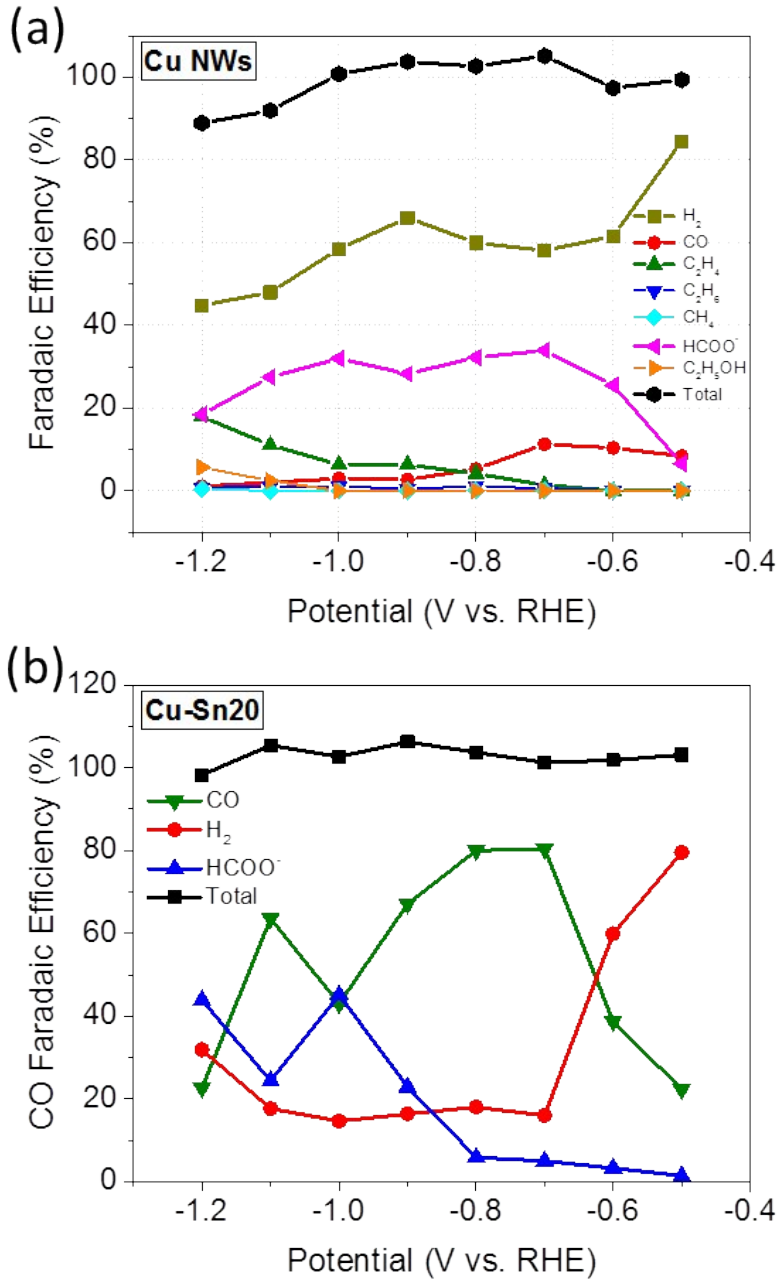

Figure S12 Product analysis of the CO_2ER on Cu NWs (a) and Cu-Sn20 NWs (b). For Cu NWs, H_2, $HCOO^-$, CO, CH_4, C_2H_4, C_2H_6 and C_2H_5OH were detected, but only H_2 and $HCOO^-$ showed a faradaic efficiency larger than 20%. For Cu-Sn20 electrode, only H_2, $HCOO^-$ and CO were detected. The sum of all the faradaic efficiency approached 100%.

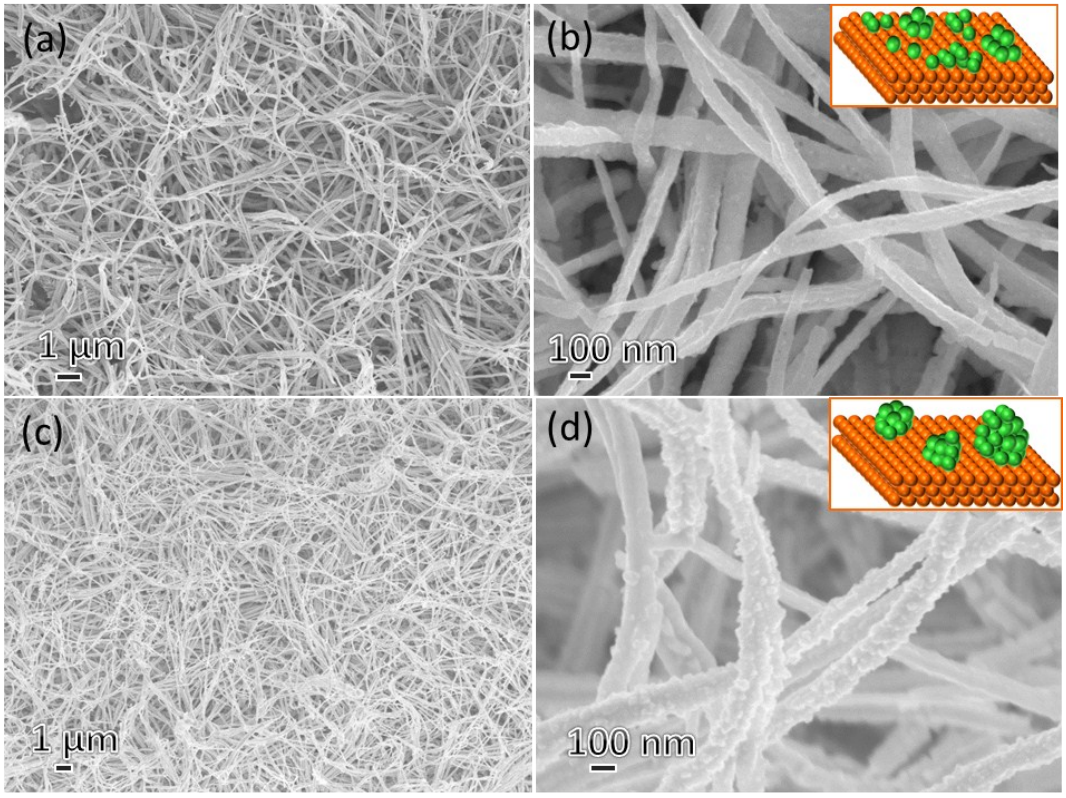

Figure S13 SEM images of the Cu-Sn20 NWs before (a, b) and after (c, d) CO_2 reduction in CO_2-satured 0.1 M $KHCO_3$ solution for 12 h at -0.8 V (vs RHE). After the prolonged bulk electrolysis, the nanowire structure remained very well. However, large amount of nanoparticles were formed on the hybrid nanowire surface. It may arise from the aggregation of Sn nanocrystals on the surface of Cu NWs during the electrolysis, as illustrated in the schematics in figure (b) and (d). With the increasing aggregation of Sn NPs, more and more Cu active sites that facilitates the H_2 generation were released, which may lead to the decay of FE_{CO} and the increase of FE_{H2} as shown in Figure 4d.

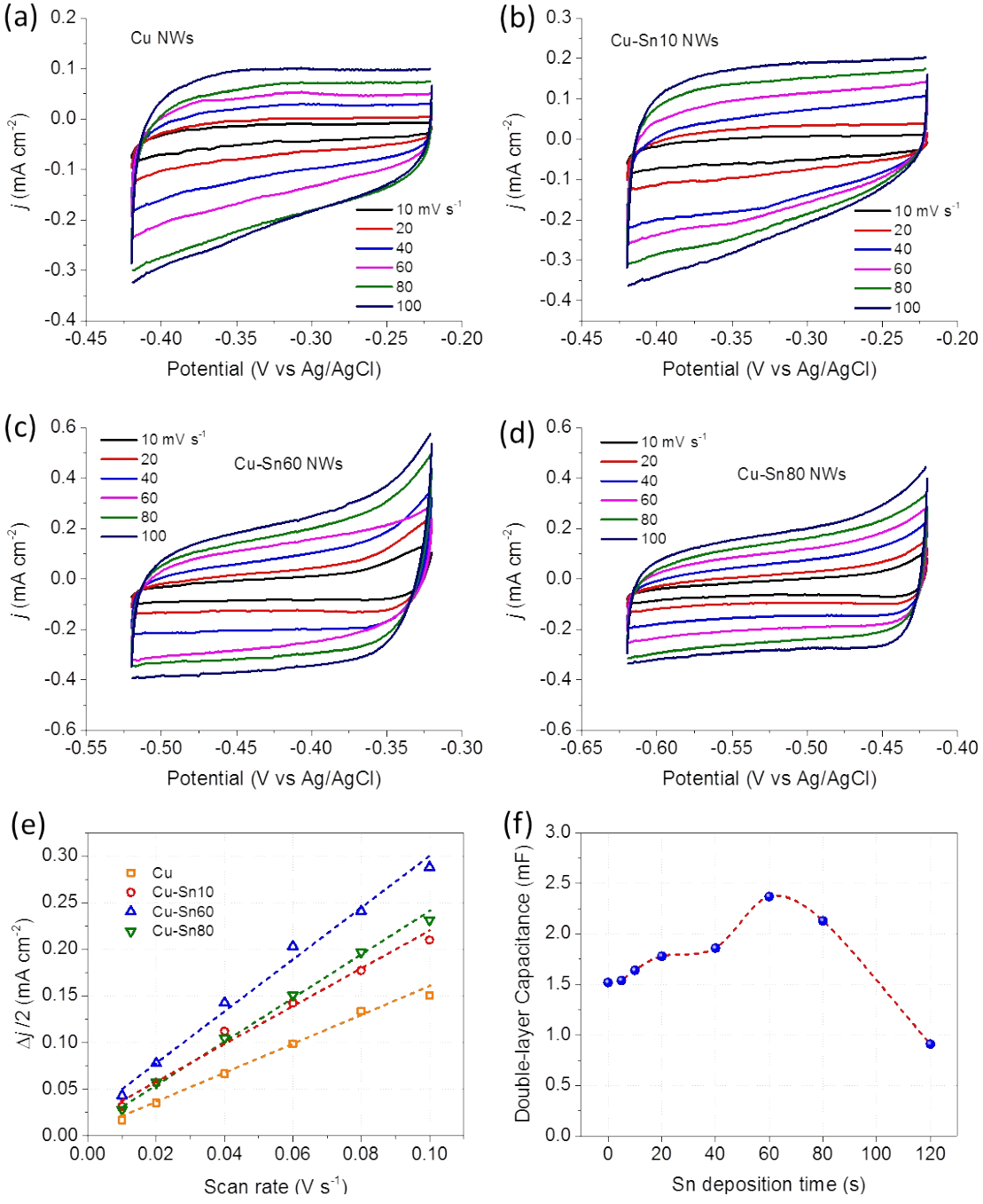

Figure S14 Determination of double-layer capacitance (C_{dl}) of Cu NWs and Cu-Sn NWs in Ar-saturated 0.1 M $HClO_4$ solution. CVs were taken over a range of scan rates in a potential window where only double-layer charging and discharging is relevant. The C_{dl} was estimated by plotting the $\Delta j/2$ against scan rates, in which the slope was C_{dl}. The Δj is the difference between j_a and j_c, where j_a and j_c are the anodic and cathodic current density at the midpoint of applied potential window, respectively.

Table S1 C_{dl} values of the Cu NWs and different Cu-Sn NWs.

Samples	C_{dl} (mF)
Cu NWs	1.52
Cu-Sn5	1.54
Cu-Sn10	1.64
Cu-Sn20	1.78
Cu-Sn40	1.86
Cu-Sn60	2.37
Cu-Sn80	2.13
Cu-Sn120	0.91

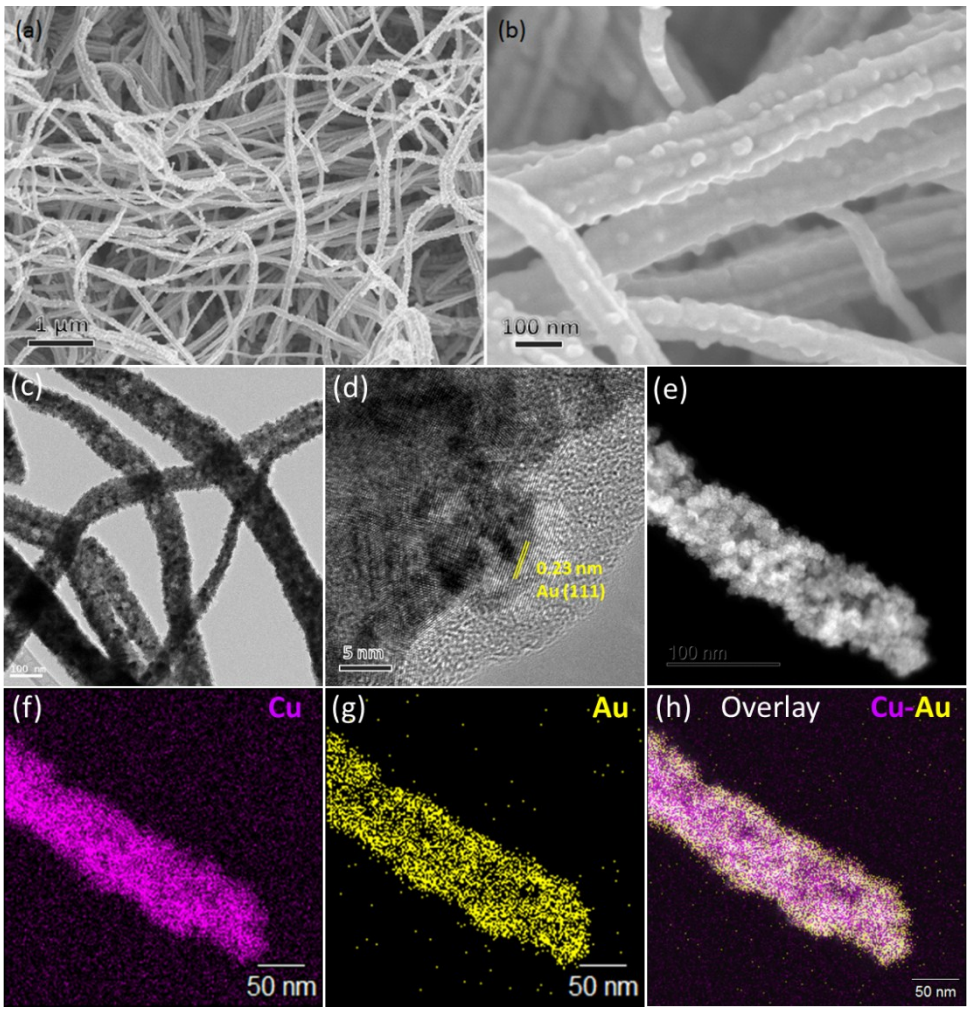

Figure S15 (a-b) SEM images of Cu-Au20 NWs under different magnifications; TEM image (c), HRTEM image (d), HAADF-STEM image and the corresponding elemental mappings (e-h) of the Cu-Au20 NWs. From the SEM images, some big gold NPs (20 ~ 100 nm) can be observed on the surfaces of the NWs. From the TEM analysis, it can be seen that the gold layer on the surfaces of Cu NWs consists of large amount of small gold nanocrystals (< 10 nm), uniformly decorating the Cu NW.

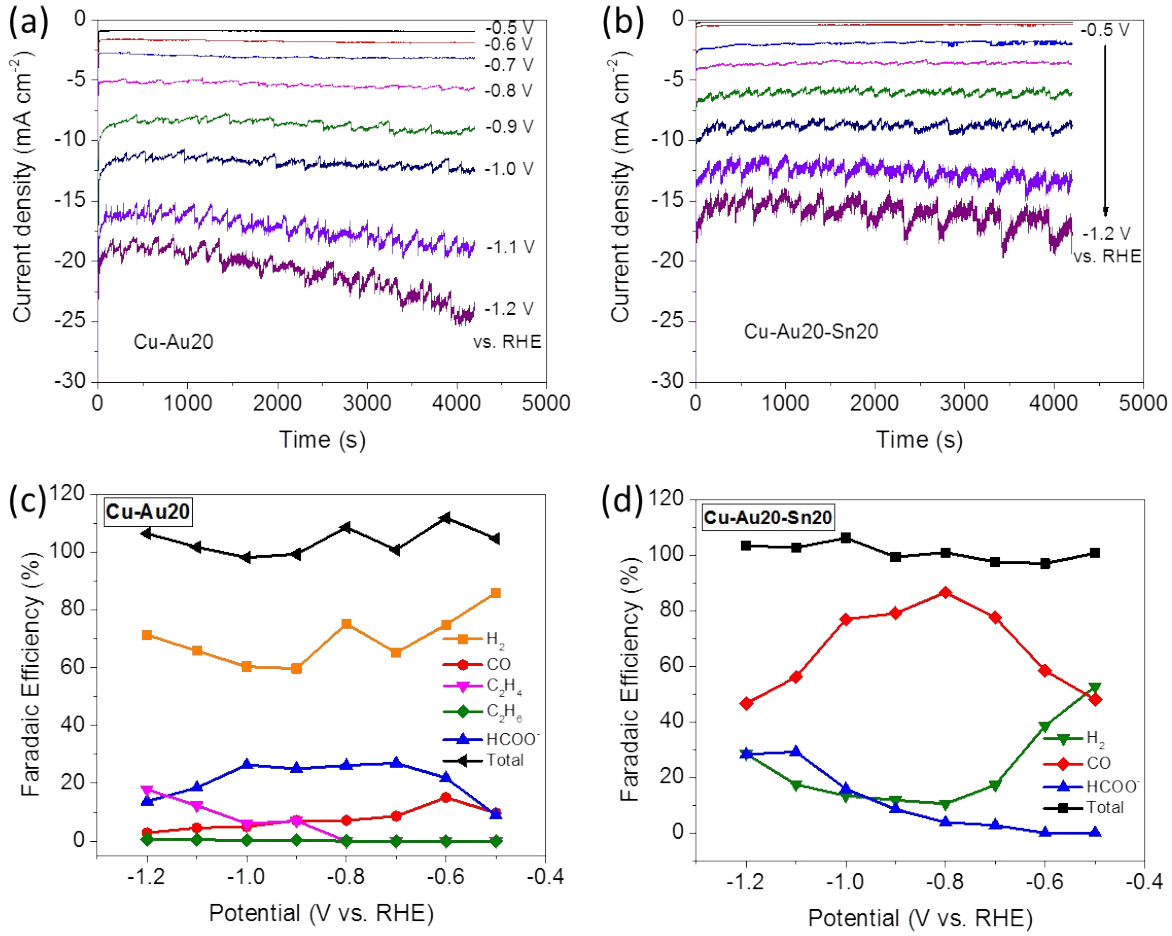

Figure S16 Chronoamperometry curves at various potentials in CO_2-satured 0.1 M $KHCO_3$ solution and the corresponding product analysis for Cu-Au20 NWs (a, c) and Cu-Au20-Sn20 NWs (b, d). For Cu-Au20 NWs, H_2, $HCOO^-$, CO, C_2H_4, C_2H_6 and C_2H_5OH (trace amount) were detected, which is almost same with the polycrystalline Cu NWs. It indicates that the introduction of gold did not obviously change the product selectivity of Cu NWs. After a rapid Sn modification of 20 s on the Cu-Au20 NWs, the FE_{CO} was intensely increased, while the FE_{H2} was evidently depressed. This is almost same to the effect on bare Cu NWs.

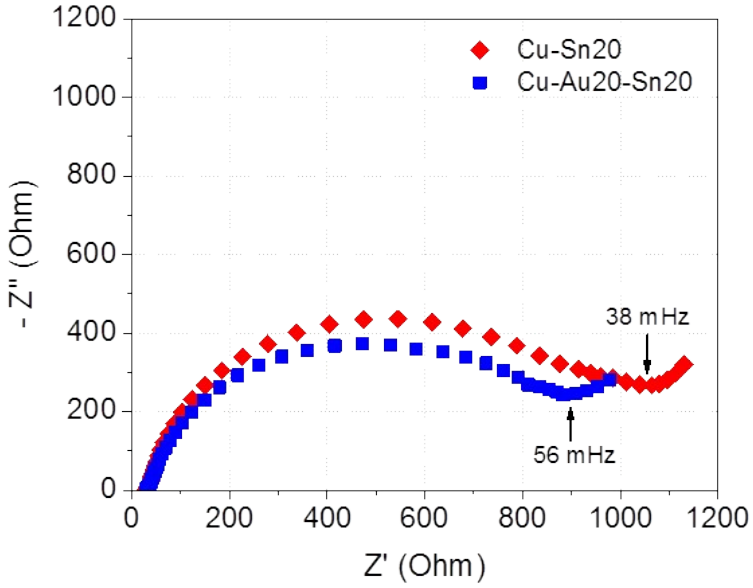

Figure S17 Electrochemical impedance spectroscopy (EIS) investigation of Cu-Sn20 NWs and Cu-Au20-Sn20 NWs in CO_2-saturated 0.1 M $KHCO_3$ solution. It was performed by applying an AC voltage with 5 mV amplitude in a frequency range from 20 mHz to 100 kHz.

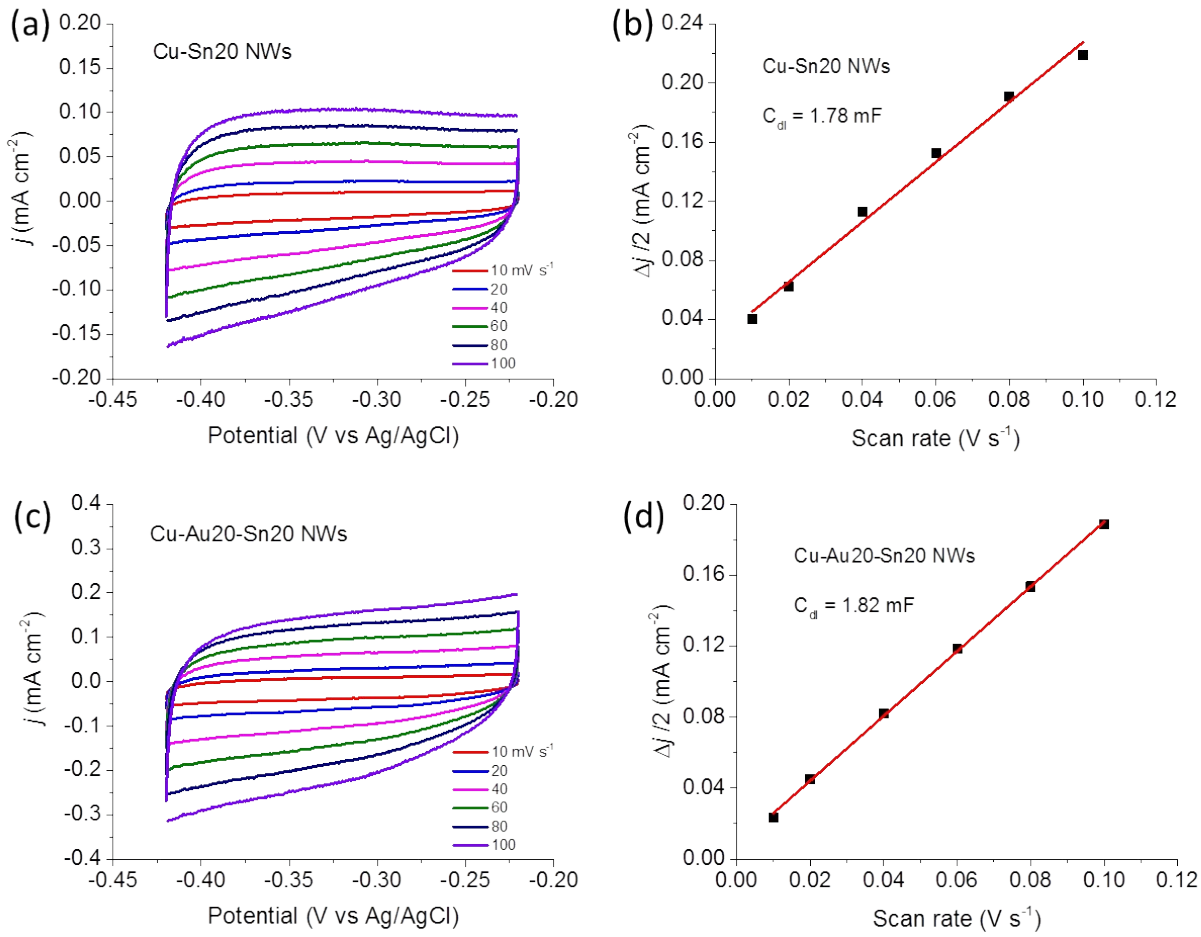

Figure S18 Comparison of the double-layer capacitances for Cu-Sn20 NWs and Cu-Au20-Sn20 NWs in Ar-saturated 0.1 M $HClO_4$ solution. The C_{dl} value of Cu-Au20-Sn20 NWs is slightly larger than that of Cu-Sn20 NWs. It indicates that the electrochemical active surface area was improved after introducing gold layer.